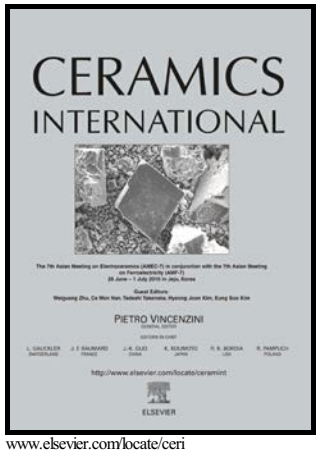

www.elsevier.com/locate/ceri

Preparation and characterization of novel nonstoichiometric magnesium aluminate spinels

Yudong Li, Dongyan Yang, Chenguang Liu, Pan yang, Pengcheng Mu, Juan Wen, Shuangqiang Chen, Yuhong Li

PII: S0272-8842(18)31293-8
DOI: https://doi.org/10.1016/j.ceramint.2018.05.145
Reference: CERI18320

To appear in: *Ceramics International*

Received date: 17 April 2018
Revised date: 15 May 2018
Accepted date: 16 May 2018

Cite this article as: Yudong Li, Dongyan Yang, Chenguang Liu, Pan yang, Pengcheng Mu, Juan Wen, Shuangqiang Chen and Yuhong Li, Preparation and characterization of novel nonstoichiometric magnesium aluminate spinels, *Ceramics International,* https://doi.org/10.1016/j.ceramint.2018.05.145

Preparation and characterization of novel nonstoichiometric magnesium aluminate spinels

Yudong Li, Dongyan Yang, Chenguang Liu, Pan yang, Pengcheng Mu, Juan Wen, Shuangqiang Chen, Yuhong Li*

School of Nuclear Science and Technology, Lanzhou University, Lanzhou 730000, China

Abstract

Magnesium aluminate spinel is of great importance for nuclear industry, and its structure, showing a great impact on properties, is sensitive to the composition. In order to explore the stoichiometric effect on structure and properties of spinels, several different spinel compositions with $MgO \cdot nAl_2O_3$ (n = 0.5-2.4) were synthesized via solid state reaction. Synthetic samples were characterized by X-ray diffraction, scanning electron microscope and nanoindentation tests. The results of XRD and SEM indicate that the single-phase magnesia alumina spinels have been prepared successfully for the first time ranging from n = 0.667 to n = 1.5, which is beyond the previous reported ranges of $n \geq 0.91$. The hardness and modulus decrease with increasing n, implying further that the nonstoichiometric spinel crystal structures are likely to exhibit superior mechanical properties.

Keywords: $MgO{\cdot}nAl_2O_3$ ceramics; Solid state reaction; Phase structure; Mechanical properties

1. Introduction

Magnesium aluminate spinels ($MgO{\cdot}nAl_2O_3$) are well known as their excellent properties and attracts considerable attention. Synthetic $MgAl_2O_4$ ($MgO{\cdot}Al_2O_3$) spinel is a high potential ceramic material for various applications [1, 2]. There are additional advantages for spinel ceramics due to the cubic crystal structure, e.g. highly radiation resistance and other highly versatile properties [3, 4]. Numerous studies have been performed to explain the excellent radiation resistance of stoichiometric spinels, in terms of large defect clusters, cation disordering, high recombination rates of vacancy-interstitial and so on [5-9]. And the intrinsic cation vacancies do play a very important role in the radiation behavior of spinels. In the ideal stoichiometric spinel ($MgAl_2O_4$) structure, Mg^{2+} occupies the tetrahedral sites and Al^{3+} occupies octahedral sites, respectively, but the cation sublattice of the spinel is not completely dense. Moreover, previous studies have shown that stoichiometry would have an important effect on the properties of spinels [10, 11]. For nonstoichiometric spinels, including the magnesia rich and alumina rich compositions, a large number of structural vacancies will be introduced, which leads to the formation of defects with different types and concentrations as

compared with stoichiometric ones. Besides, stoichiometric and nonstoichiometric spinels are of great importance for various applications [12] .

These studies, however, was just focused on $MgO{\cdot}nAl_2O_3$ with the compositions of $n \geq 1$ [9, 13, 14], and few people have paid attention to the magnesia rich compounds ($n < 1$). According to the temperature-composition (T-C) phase diagram of $MgO\text{-}Al_2O_3$ binaries [15], showing as Fig. 1, one can find that it is difficult to synthesize the magnesia rich spinels at relatively low temperatures. Efforts have been devoted to the synthesis of $MgO{\cdot}nAl_2O_3$ ($n < 1$) compositions from the oxide precursors of Al_2O_3 and MgO, and single-phases with $MgO{\cdot}nAl_2O_3$ compositions extends from $n = 0.91$ at 1600 ^{o}C were obtained [15, 16]. During solid state reaction, there are some limiting factors for spinel preparation, such as the reactivity of raw materials, sintering temperatures and so on [12].

In order to get a deeper understanding of the magnesia rich spinel compounds ($n < 1$), we have tuned the experimental conditions of solid state reaction based on previous works to complete the reaction, such as the holding time at the maximum temperature and a suitable sintering profile. We tried to synthesis the $MgO{\cdot}nAl_2O_3$ ceramics with n ranging from 0.5 to 2.4 according to the phase diagram [15]. Synthetic samples were characterized by X-ray diffraction and scanning electron microscope. Moreover, nanoindentation tests were carried out to measure the hardness and elastic modulus of as-prepared products, which are two major factors to describe the mechanical properties of materials. Both parameters are great high for ceramic materials [17-20].

2. Experimental Procedure

2.1. Sample preparation

The $MgO{\cdot}nAl_2O_3$ (n = 0.5, 0.667, 0.85, 1, 1.25, 1.5, 1.75, 2.4) ceramics were synthesized by solid state reaction method. The starting powders are commercially available MgO and Al_2O_3 (99.99% of purity) with particle diameter above 40nm (HW-Technik, Beijing, China). The stoichiometric constituents of $MgO{\cdot}nAl_2O_3$ were mixed by ball-milling for 6 h (5 h for planetary ball mill and 1 h for single-phase asynchronous motor). The well milled powders were then pressed into pellets under the pressure of 16 MPa with 3 min holding time. Finally, the pressed pellets were sintered at 1200 ^{o}C for 24 h in an air atmosphere, with a heating rate of 5 ^{o}C/min and a cooling rate of 10 ^{o}C/min. The calcined samples were again ball-milled for 6 hours, then pressed into pellets. The resultant products were heated by a rate of 5 ^{o}C/min up to 1000 ^{o}C (keeping 6 h), followed by a heating of 3 ^{o}C/min up to 1600 ^{o}C （keeping 72 h).

2.2. Structure characterization

The phase structure of the synthesized samples was determined by X-ray diffraction (X'Pert Pro, PANalytical, Netherlands) with Cu Ka radiation (λ_1 = 0.154060 nm and λ_2 = 0.154443 nm). The lattice parameters were calculated by a slow scanning XRD over the range 10-90° with the rate of 0.02° per second. The microstructure of the ceramics was examined by a scanning electron microscope

(SEM, JSM-5600LV, Electronic Optical, Japan) attached with backscatter electron (BSE) probe and energy dispersive spectrometer (EDS) facility. The porosities of sintered pellets were calculated using the bulk density and theoretical density.

2.3. Mechanical properties measurement

The nanoindentation experiments were carried out using a Nano Indenter G200 with a diamond Berkovich indenter. During the indentation experiment, a continuous stiffness measurement, superposed with a small dynamic cyclic loading on the previous technology, was applied, shown in Fig. 2. The nanoindentation tip was stationary and the sample was driven closer to the tip in a movement no more than 0.5 nm. In this study, a maximum depth of 900 nm and a maximum load of 280 mN were set to avoid tip damage. Five different point in each tested sample were selected.

3. Results and Discussion

3.1. Phase confirmation

The XRD patterns of the $MgO{\cdot}nAl_2O_3$ (n = 0.5, 0.667, 0.85, 1, 1.25, 1.5, 1.75, 2.4) compounds sintered at 1600 ^oC are shown in Fig. 3. $MgO{\cdot}nAl_2O_3$ (n = 0.667, 0.85, 1, 1.25, 1.5) compositions exhibit a pure spinel structure, which is characterized by the presence of superstructure peaks marked in the XRD pattern. Additional peaks, marked with "*" in $MgO{\cdot}1.75Al_2O_3$ and $MgO{\cdot}2.4Al_2O_3$, are the diffraction peaks corresponding to Al_2O_3 (ICDD 74-1081), and some marked with "

•" in $MgO{\cdot}0.5Al_2O_3$, corresponding to MgO (ICDD 74-1225). We also tried to prolong the holding time at the maximum temperature to make the reaction more completely, but the longer holding time did not cause significant structural changes. Therefore, we can tentatively speculate that the critical value of single-phase spinel ranges from $n = 0.667$ to $n = 1.5$ at 1600 ^{o}C.

The representative SEM image of synthesized $MgO{\cdot}nAl_2O_3$ taken in backscatter electron (BSE) mode and corresponding elemental analysis are displayed in Fig. 4. It is worth noting that we have plated a layer of gold on the surface of the samples before testing SEM because of the poor conductivity of ceramic materials. It is necessary to ignore the influence of gold in subsequent elemental analysis. Based on the BSE images, there are two different phases in $MgO{\cdot}0.5Al_2O_3$, $MgO{\cdot}1.75Al_2O_3$ and $MgO{\cdot}2.4Al_2O_3$. Elemental analysis is quite consistent with the results of BSE images. For the $MgO{\cdot}0.5Al_2O_3$ composition, it can be found that magnesium is distributed throughout the visible purview and concentrated in some areas, but there is few or no distribution of aluminum in magnesium enriched region. The magnesium enriched region almost coincides with the darker phase in BSE images. When taken together, we can consider that the dark phase represented the composition of MgO. The results of elemental analysis of bright phase show the characteristics of spinel. Therefore, the $MgO{\cdot}0.5Al_2O_3$ compound consists of two phases of magnesia and spinel, which is in good agreement with XRD results. For the compositions of 1.75 and 2.4, it is not easy to identify the difference between the two phases from BSE images, but magnesium

and aluminum are not evenly distributed. Considering these results, the two spinel compositions ($MgO{\cdot}1.75Al_2O_3$ and $MgO{\cdot}2.4Al_2O_3$) both consist of alumina and spinel.

For the compositions ranging from n = 0.667 to n = 1.5, the results reveal that there is just a single phase (spinel) in these compositions. Combined with the XRD patterns, we can conclude that the single-phase magnesia alumina spinels have been prepared successfully ranging from n = 0.667 to n = 1.5, at 1600 ^{o}C. Comparing with the previous conclusions that the critical value extends from n = 0.91, the increased composition range of single phase nonstoichiometric spinels can be ascribed to the tuned experimental conditions. In other words, the improved experimental conditions are favorable for promoting the reaction more completely.

3.2. Structural properties

It can be seen that the XRD peaks of single-phase compounds shifts toward larger angles with increasing content of aluminum in Fig. 3. The lattice parameters of $MgO{\cdot}nAl_2O_3$ (n = 0.667, 0.85, 1, 1.25, 1.5) were calculated from the XRD patterns, and the results are presented in Fig. 5. The lattice parameter of these samples decreases with increasing n. It is easily understood since that the ionic radius of Al^{3+} is smaller than its of Mg^{2+}, and the lattice volume decreases with the increasing content of Al^{3+}. Another significant change observed is that the intensity of some reflections changes as a function of composition. The {111} reflection is particularly sensitive to the cation occupation in tetrahedral and octahedral sites.

According to the analysis of structure factors of spinels, the relatively strong {111} diffraction suggests a low degree of disorder [21]. Fig. 6 shows the intensity of {111} superstructure peak as a function of compositions from n = 0.667 to n = 1.5. The intensity of {111} diffraction increases to the maximum and then decreases whether we introduced excess aluminum or excess magnesium. In a word, the intensity of {111} diffraction is a trend of "M" type. The results indicate that the degree of disorder decreases first and then increases when we introduce excess MgO or excess Al_2O_3 to $MgO{\cdot}Al_2O_3$. There is a cation exchange phenomenon in the synthetic stoichiometric spinel. For the magnesia rich or alumina rich compositions, most of Mg^{2+} or Al^{3+} tend to occupy the tetrahedral or octahedral sites considering the ionic radius and valence, which will lead to a decrease in the ratio of cation inverse. The excess Mg^{2+} or Al^{3+} would result in an increased inverse when the tetrahedral sites of Mg^{2+} or the octahedral sites of Al^{3+} reaches a saturated amount.

Fig. 7 presents the results of porosity of sintered specimens as a function of the composition. With an increase of n from 0.667 to 1.5, the porosity of our samples was changed from 2% to 14%. According to previous studies [16], the densification rate and density decrease gradually from the MgO-rich compositions to the Al_2O_3-rich compositions, which is consistent with the results in this study.

3.3. Mechanical properties

The nanoindentation experiments were performed in $MgO{\cdot}nAl_2O_3$ (n = 0.667, 1, 1.25, 1.5). Fig. 8 shows the variation of hardness and modulus as a function of

the composition. These spinel compositions synthesized in this study exhibit a hardness of 18-21 GPa and a modulus of 300-320 GPa. Previous experiments have demonstrated that the hardness and modulus of $MgAl_2O_4$ are ~16 GPa and ~280 GPa, respectively [22, 23]. The higher values for modulus and hardness in present study confirm that our samples possess better resistance to elastic and plastic deformations. That is to say, the improved experimental conditions are beneficial to obtain the samples with the superior mechanical properties. In addition, the hardness and modulus show a tendency to decrease with increasing *n*. Generally, the grain size of materials plays a critical role in its mechanical properties, such as hardness, strength and so on [24]. Materials with smaller grain size possess larger boundary area, and the existence of grain boundary can inhibit the movement of dislocation, which leads to the increase of plastic deformation resistance. In other words, the smaller grain size causes higher hardness macroscopically. The surface morphology of the selected samples in our work is presented in Fig.9. It is noteworthy that the scale in the four picture is different. The grain size of these pellets is significantly increased with an increasing of *n* (about from 10 μm to 70 μm), which is well agreement with the results that the hardness and modulus show a tendency to decrease. Grain size may be the mainly responsible for the phenomenon. The results indicate that it is likely to present new compositions with superior mechanical properties in the $MgO{\cdot}nAl_2O_3$ crystal structure system. Besides, fracture toughness is also an important aspect of the mechanical properties of the sample, and the investigation of the fracture toughness of our samples will be carried out in

future investigations.

Conclusion

Several different spinel compositions with $MgO \cdot nAl_2O_3$ (n = 0.5, 0.667, 0.85, 1, 1.25, 1.5, 1.75, 2.4) were synthesized by solid state reaction at 1600 ^{o}C. The improved experimental conditions were applied. Experimentally, we can confirm that the single-phase nonstoichiometric spinels were achieved ranging from n = 0.667 to n = 1.5, based on XRD and SEM characterization. In addition, the nanoindentation experiments were performed to test its mechanical properties. The results presented here reveal that the improved experimental conditions lead to the samples of better mechanical properties. The hardness and modulus decrease as n increases, implying further that there would be new compositions with superior mechanical properties in the ranges of $n < 1$.

Acknowledgements

This work was sponsored by the National Natural Science Foundation of China (11775102 and 11475076) and the Fundamental Research Funds for the Central Universities of China (Lanzhou University, lzujbky-2017-14).

References

[1] N. Chauvin, R.J.M. Konings, H. Matzke, Optimisation of inert matrix fuel concepts for americium transmutation, J. Nucl. Mater, 274 (1999) 105-111.

[2] E.A.C. Neeft, R.J.M. Konings, K. Bakker, J.G. Boshoven, H. Hein, R.P.C. Schram, A. van Veen, R. Conrad, Neutron irradiation of polycrystalline yttrium aluminate garnet, magnesium aluminate spinel and α-alumina, J. Nucl. Mater, 274 (1999) 78-83.

[3] K. Yasuda, T. Yamamoto, M. Shimada, S. Matsumura, Y. Chimi, N. Ishikawa, Atomic structure and disordering induced by 350 MeV Au ions in $MgAl_2O_4$, Nucl. Instrum. Meth. B, 250 (2006) 238-244.

[4] N.W. Grimes, The spinels: versatile materials, Physics in Technology, 6 (1975) 22.

[5] C. Kinoshita, S. Matsumura, K. Yasuda, T. Soeda, M. Noujima, Irradiated Microstructures of Magnesium Aluminate Spinel and their Controlling Factors, MRS Proceedings, 540 (2011) 287.

[6] C. Kinoshita, K. Fukumoto, K. Fukuda, F.A. Garner, G.W. Hollenberg, Why is magnesia spinel a radiation-resistant material? J. Nucl. Mater, 219 (1995) 143-151.

[7] S.J. Zinkle, Effect of irradiation spectrum on the microstructural evolution in ceramic insulators, J. Nucl. Mater, 219 (1995) 113-127.

[8] K. Yasuda, C. Kinoshita, Electron-beam induced dissociation of dislocation loops in magnesia–alumina ceramics, Nucl. Instrum. Meth. B, 191 (2002) 559-564.

[9] K.E. Sickafus, N. Yu, M. Nastasi, Radiation resistance of the oxide spinel: the role

of stoichiometry on damage response, Nucl. Instrum. Meth. B, 116 (1996) 85-91.

[10] K.E. Sickafus, A.C. Larson, N. Yu, M. Nastasi, G.W. Hollenberg, F.A. Garner, R.C. Bradt, Cation disorder in high dose, neutron-irradiated spinel, J. Nucl. Mater, 219 (1995) 128-134.

[11] K. Yasuda, C. Kinoshita, R. Morisaki, H. Abe, Role of irradiation spectrum in the microstructural evolution of magnesium aluminate spinel, Philos. Mag. A, 78 (1998) 583-598.

[12] R. Sarkar, G. Bannerjee, Effect of addition of TiO_2 on reaction sintered MgO-Al_2O_3 spinels, J. Eur. Ceram. Soc, 20 (2000) 2133-2141.

[13] T. Soeda, S. Matsumura, C. Kinoshita, N.J. Zaluzec, Cation disordering in magnesium aluminate spinel crystals induced by electron or ion irradiation, J. Nucl. Mater, 283-287 (2000) 952-956.

[14] K.E. Sickafus, N. Yu, R. Devanathan, M. Nastasi, The irradiation damage response of $MgO \cdot 3Al_2O_3$ spinel single crystal under high-fluence ion-irradiation, Ion Beam Modification of Materials, Elsevier, Amsterdam, 1996, pp. 573-578.

[15] B. Hallstedt, Thermodynamic Assessment of the System MgO-Al_2O_3, J. Am. Ceram. Soc, 75 (2005) 1497-1507.

[16] C.J. Ting, H.Y. Lu, Defect Reactions and the Controlling Mechanism in the Sintering of Magnesium Aluminate Spinel, J. Am. Ceram. Soc, 82 (2004) 841-848.

[17] R.C. Bradt, D. Munz, M. Sakai, K.W. White, Fracture Mechanics of Ceramics: Active Materials, Nanoscale Materials, Composites, Glass and Fundamentals, Gastroenterol. Clin. N, 16 (1987) 511-515.

[18] A. Cutler Raymond, J. Mayhew Robert, M. Prettyman Kevin, V. Virkar Anil, High-Toughness Ce-TZP/Al_2O_3 Ceramics with Improved Hardness and Strength, J. Am. Ceram. Soc, 74 (2005) 179-186.

[19] G. Fantozzi, G. Orange, K. Liang, M. Gautier, J.P. Duraud, P. Maire, C. Gressus, E. Gillet, Effect of Nonstoichiometry on Fracture Toughness and Hardness of Yttrium Oxide Ceramics, J. Am. Ceram. Soc, 72 (2005) 1562-1563.

[20] W. Rice Roy, C. Wu Carl, F. Boichelt, Hardness-Grain-Size Relations in Ceramics, J. Am. Ceram. Soc, 77 (2005) 2539-2553.

[21] M. Tang, J.A. Valdez, Y. Wang, J. Zhang, B.P. Uberuaga, K.E. Sickafus, Ion irradiation-induced crystal structure changes in inverse spinel $MgIn_2O_4$, Scripta. Mater, 125 (2016) 10-14.

[22] R. Devanathan, N. Yu, K.E. Sickafus, M. Nastasi, Structure and mechanical properties of irradiated magnesium aluminate spinel, J. Nucl. Mater, 232 (1996) 59-64.

[23] O. Tokariev, R.W. Steinbrech, L. Schnetter, J. Malzbender, Micro- and macro-mechanical testing of transparent $MgAl_2O_4$ spinel, J. Mater. Sci, 47 (2012) 4821-4826.

[24] O. Tokariev, L. Schnetter, T. Beck, J. Malzbender, Grain size effect on the mechanical properties of transparent spinel ceramics, J. Eur. Ceram. Soc, 33 (2013) 749-757.

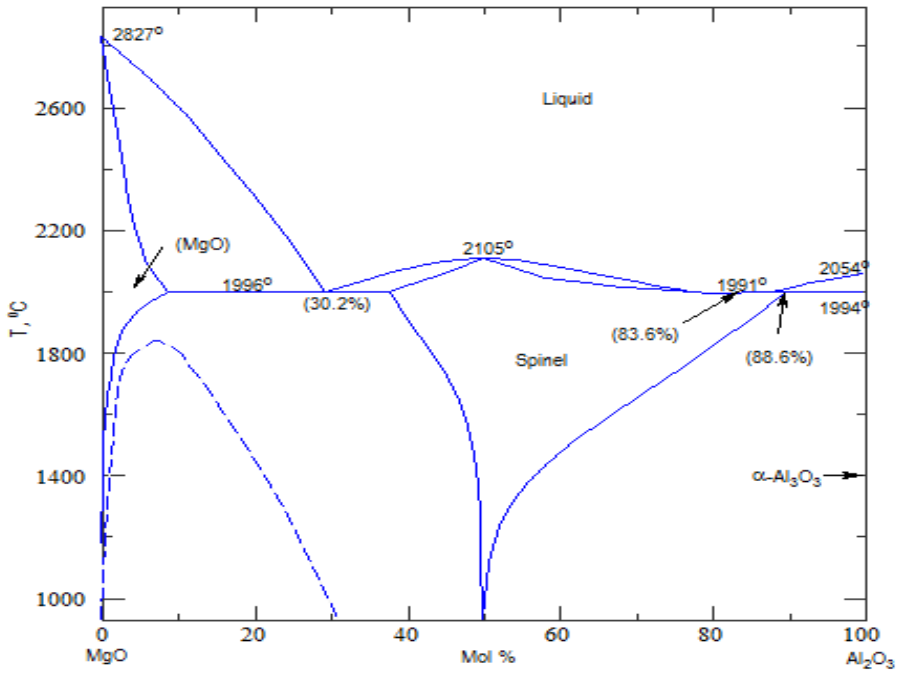

Fig. 1. The T-C phase diagram of MgO-Al_2O_3 binaries [15]. The area of single-phase spinel is only a small part. It is particularly difficult to synthesize the nonstoichiometric ($n < 1$) spinel.

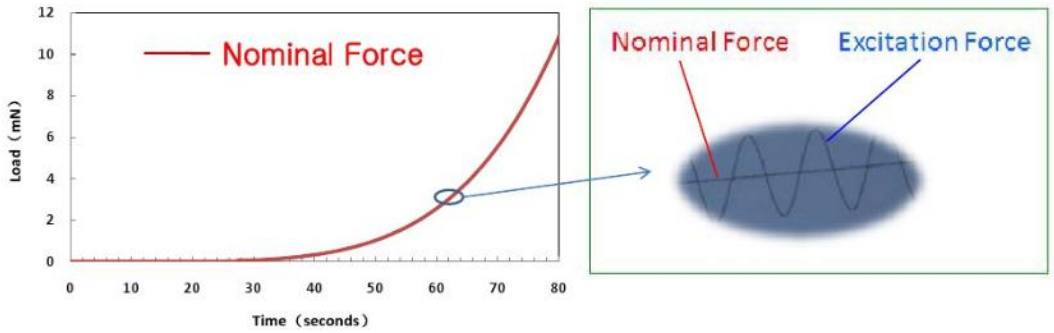

Fig. 2. The indentation load force of quasi static and continuous stiffness measurement.

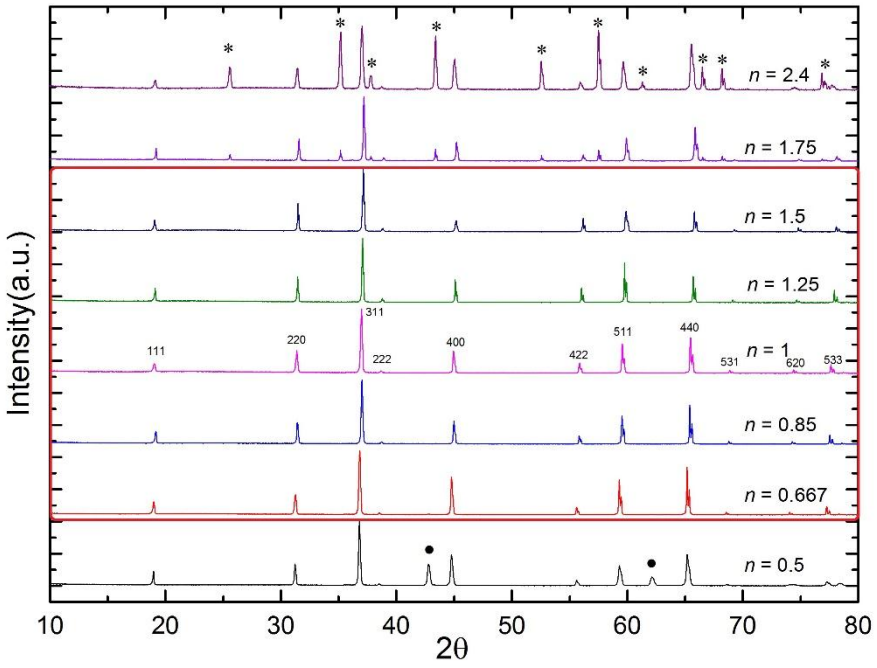

Fig. 3. XRD characterization of different spinel compositions. These figures from the bottom to the top correspond to the compositions from n = 0.5 to n = 2.4. The compositions of single-phase spinel range from n = 0.667 to n = 1.5 at 1600 ^{o}C.

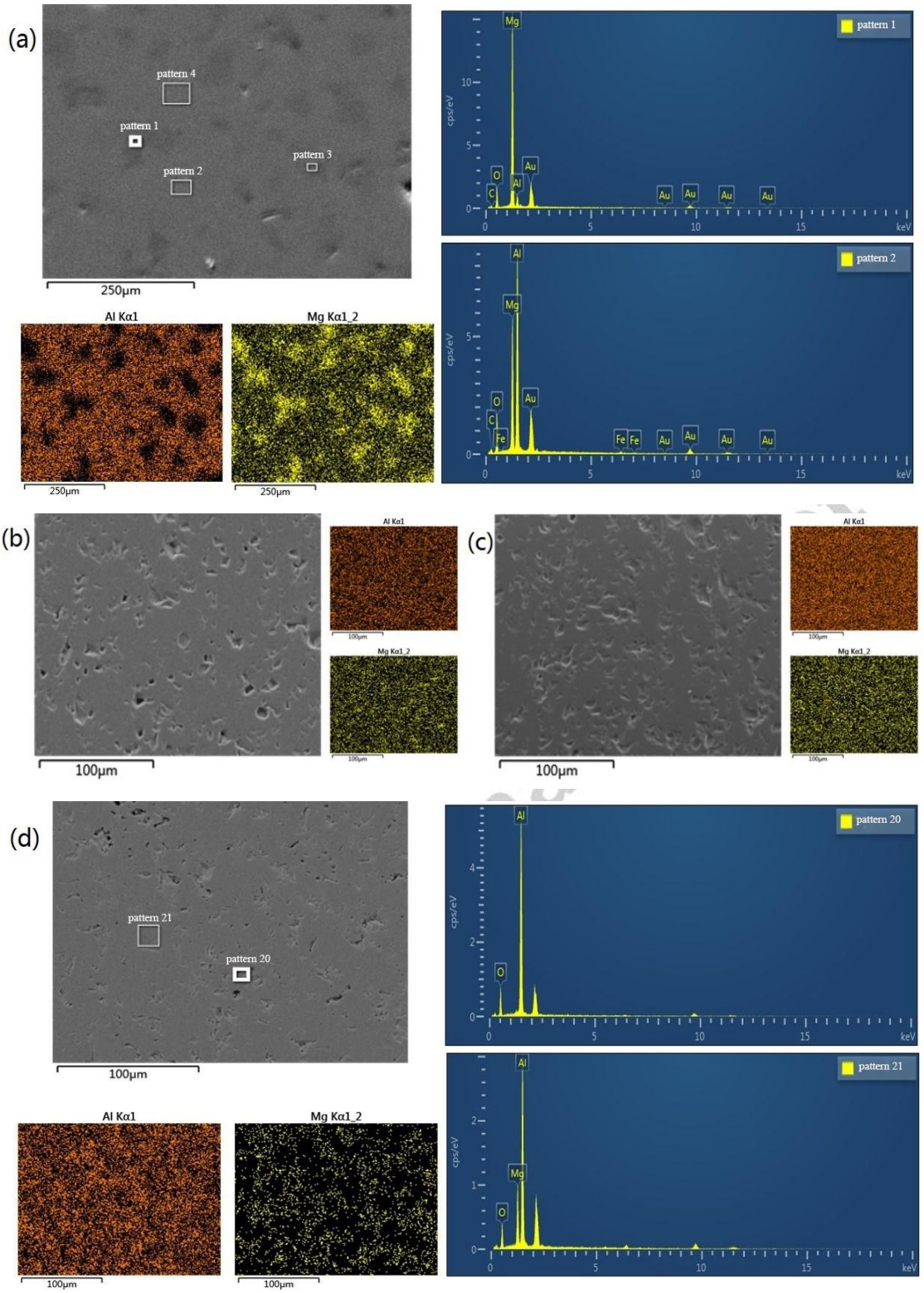

Fig. 4. The SEM backscatter electron images and elemental analysis of several spinel compositions. (a) n = 0.5; (b) n = 0.667; (c) n = 1.5; (d) n = 1.75. For the $MgO{\cdot}0.5Al_2O_3$ and $MgO{\cdot}1.75Al_2O_3$, the elements were not uniformly distributed and there were some areas where

elements were enriched, and so did the $MgO{\cdot}2.4Al_2O_3$. For the compositions from n = 0.667 to n = 1.5, there was not an observation of the enrichment of elements.

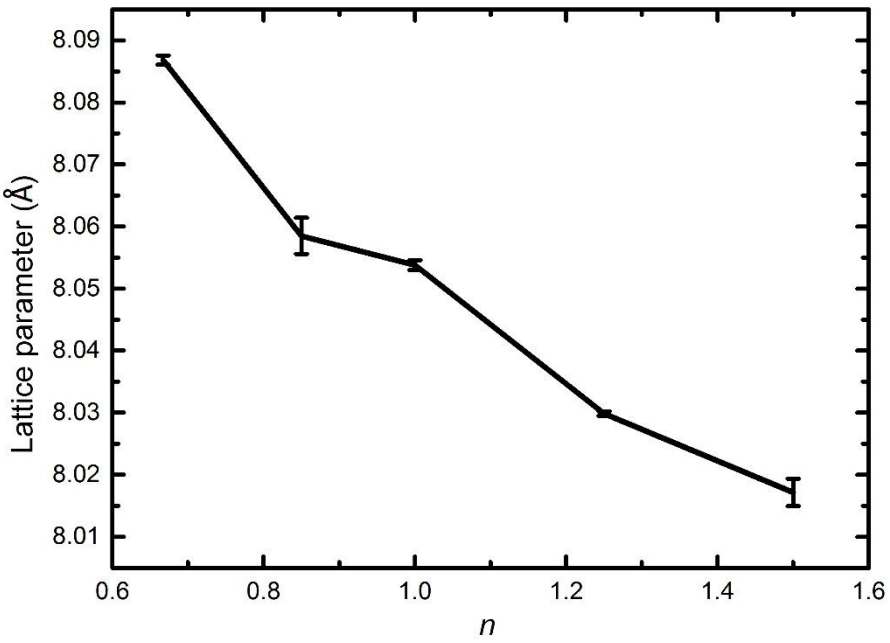

Fig. 5. Trend of lattice parameter with the compositions. The peak position shifts toward large angles in XRD, representing the decrease of the lattice parameter.

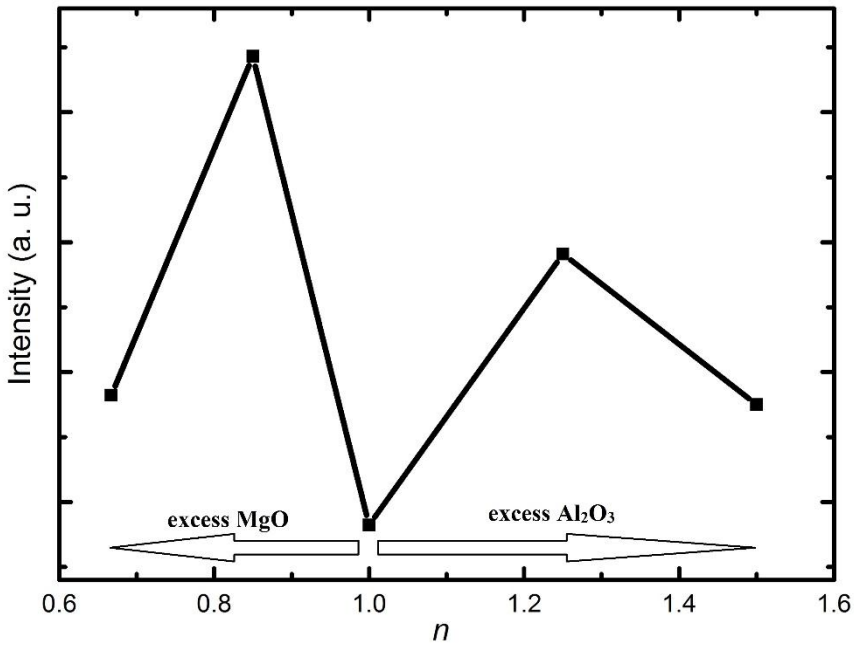

Fig. 6. The normalization intensity of {111} reflection. The intensity of {111} diffraction increases to the maximum and then decreases with the compositions whether we introduced excess aluminum or excess magnesium. The intensity of {111} diffraction is a trend of "M" type.

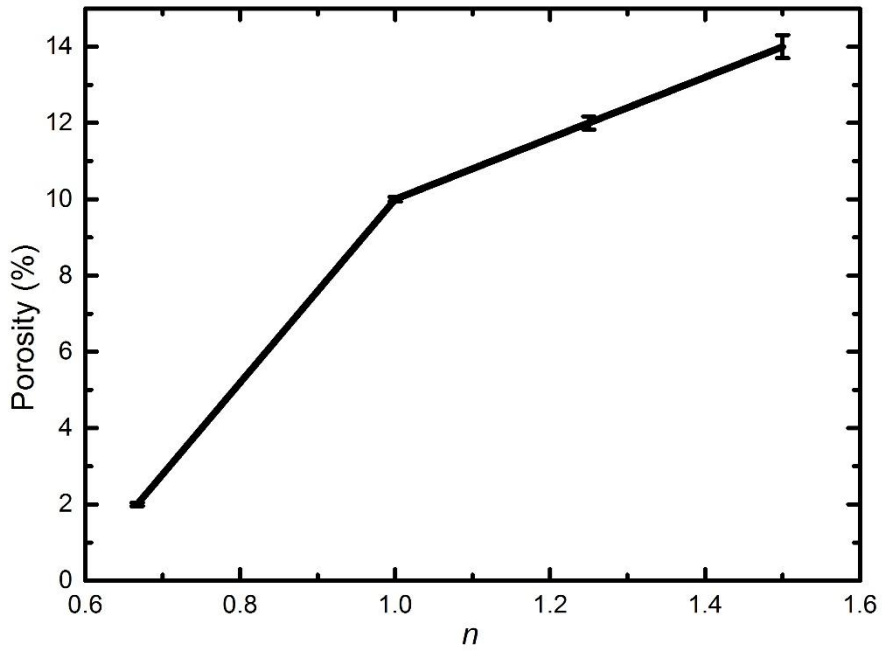

Fig. 7. The variation of the porosity of sintered specimens as a function of the composition.

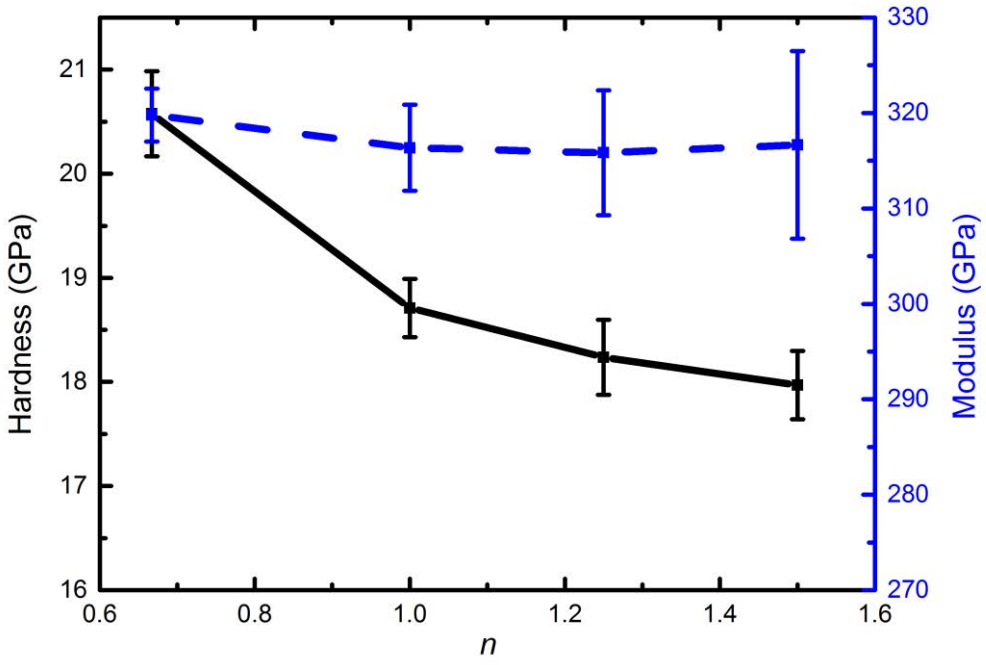

Fig. 8. The trend of hardness and modulus with the compositions. The two parameters overall present a decreasing trend.

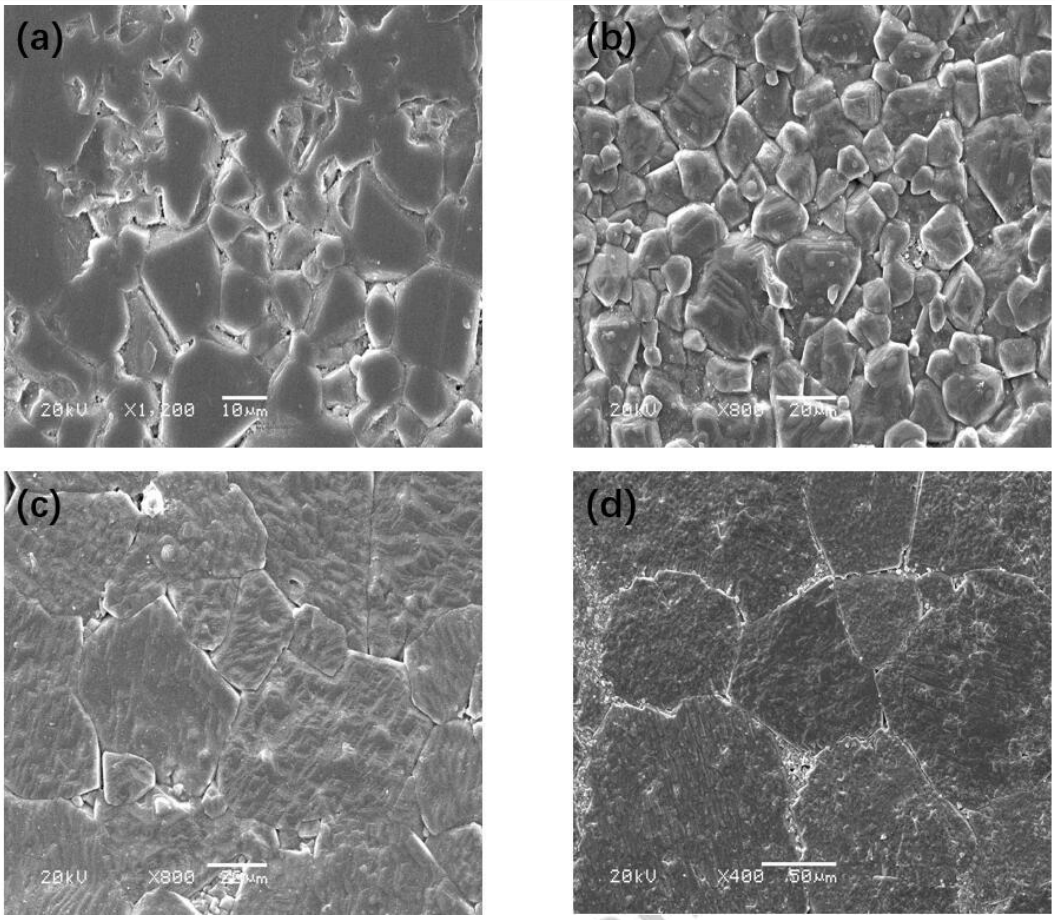

Fig. 9. Surface morphology of sintered pellets of representative samples (a) n = 0.667, (b) n = 1, (c) n = 1.25 and (d) n = 1.5. The grain size of these pellets is significantly increased with an increasing of n